Not Only Enthalpy: Large Entropy Contribution to Ion Permeation Barriers in Single-File Channels

Guillem Portella, Jochen S. Hub, Martin D. Vesper, and Bert L. de Groot
Computational Biomolecular Dynamics Group, Max-Planck-Institute for Biophysical Chemistry, Göttingen, Germany

ABSTRACT The effect of channel length on the barrier for potassium ion permeation through single-file channels has been studied by means of all-atom molecular dynamics simulations. Using series of peptidic gramicidin-like and simplified ring-structured channels, both embedded in model membranes, we obtained two distinct types of behavior: saturation of the central free energy barriers for peptidic channels and a linear increase in simplified ring-structured channels with increasing channel length. The saturation of the central free energy barrier for the peptidic channels occurs at relatively short lengths, and it is correlated with the desolvation from the bulk water. Remarkably, decomposition of free energy barriers into enthalpic and entropic terms reveals an entropic cost for ion permeation. Furthermore, this entropic cost dominates the ion permeation free energy barrier, since the corresponding free energy contribution is higher than the enthalpic barrier. We conclude that the length dependence of the free energy is enthalpy-dominated, but the entropy is the major contribution to the permeation barrier. The decrease in rotational water motion and the reduction of channel mobility are putative origins for the overall entropic penalty.

INTRODUCTION

Ion channels, located in lipid membranes that isolate organelles and cells, allow the passage of ions from one side of a membrane to the other. Their structure and composition is diverse, although they share some characteristics, such as hydrophilic lumens composed of peptide backbone carbonyl groups and a narrow selectivity filter (1). Their function affects electrochemical gradients, and thus ion channels play a fundamental role in the energetics of living cells. A subtle balance of ion gradients is, for example, responsible for the polarization-depolarization of neurons that leads to electrical signal transmission in nerve cells (2). Ion channels evolved to be selective (3), either to single ionic species like potassium (4–8) or to a certain class of ions; e.g., gramicidin only allows the passage of small univalent cations (9,10).

Additionally, molecular channels play an essential role in nanotechnology. Accurate knowledge of their structure-activity relationship is prerequisite to designing fine-tuned channels that permeate selectively, allow the detection of ligand-protein interactions (11,12), or monitor chemical reactions (13).

To gain understanding in the relationship between ionic permeation characteristics and the physical determinants underlying permeation in ion channels, we carried out a systematic study using simplified model pores. Previous work thoroughly described the effects of channel radius, surface character, and flexibility on the permeation of water and ions through model channels (14,15). Here we focused on the effect of the channel length on the permeation of potassium ions across single-file channels.

An atomistic description of the system is required to understand the interactions involved in ion permeation. The use of molecular dynamics (MD) simulations together with an all-atom force field establishes a balanced compromise between accuracy and sampling power. Nevertheless, due to the long timescales required to observe spontaneous passage of ions (2), direct calculations of ion fluxes are not feasible. The use of strong forces or large membrane potentials to impose ion permeations would introduce conditions that differ from experimental or physiological conditions (16). Here, we will concentrate on the thermodynamic function that characterizes systems in equilibrium, i.e., the free energy. Since we are interested in the passage of ions across the main pore axis, we extract free energy profiles for ion permeation in the form of potentials of mean force (PMF) (17) as a means of comparing energetic costs for ion permeation. The PMF can be used as basis for coarse-grained theories of ion conductance (18,19).

Electrostatic interactions are fundamental components of ion permeation. Therefore, methods such as continuum-electrostatic Poisson-Boltzmann calculations are routinely used to study the energetics of ion permeation. However, these methods may suffer from limitations because they do not explicitly account for the behavior of individual water molecules (20), and effects arising from channel flexibility (21,22). Here, we present free energy profiles from atomistic, explicit solvent MD simulations that take these effects particularly into account. From these simulations, we extracted the thermodynamic components of the free energy, the enthalpy, and the entropy, to quantify their contribution to the resulting transport barrier.

THEORY AND METHODS

Design and setup

A series of D,L polyalanine peptides with increasing length and a β-helix gramicidin A folding motif were used to study the energetics of potassium

Submitted January 29, 2008, and accepted for publication May 9, 2008.

Address reprint requests to Bert L. de Groot, Tel.: 49-551-201-2308; E-mail: bgroot@gwdg.de.

Editor: Peter C. Jordan.

0006-3495/08/09/2275/08 $2.00

doi: 10.1529/biophysj.108.130609

ion permeations in peptidic environments (Fig. 1, *a* and *a′*). The modeling of the polyalanine peptides was done as previously described (23). In short, a monomer of the gramicidin A channel in the head-to-head helical conformation was used to construct shorter and longer channels. The template structure has all residues mutated to alanine to achieve high regularity among the channels. The mutated gramicidin monomer, p-15, was elongated or shortened in steps of two residues. The studied peptidic channels range from p-11 to p-31, which spans a length between 0.8 and 2.6 nm. Soft position restraints (500 kJ/mol/nm^2) on the peptide backbone and termini capping groups, formyl and ethanolamine, ensure that peptides remain in the β-helix fold and have a well-defined access to the channel. To isolate the effect of the channel length, matching membranes were constructed using octane molecules (Fig. 1 *a″*), as described before (23). Unwanted deviations in the adjustment of the membrane-peptide interface can give rise to different contributions of the ion-solvent interaction to ion permeation. Since ion-water interactions are key energetic components, special care must be taken in adjusting the membrane thickness to ensure consistency over the studied systems. To ensure a stable octane slab, we used pressure coupling only in the *xy* plane, normal to the channel main axis.

A second set of systems (ring-05), built of artificial ring-structured channels, was also studied (Fig. 1, *b* and *b′*). The channel setup was inspired by a design of Crozier et al. (24). The rings, consisting of alternating carbonlike and oxygenlike particles, were connected with bonds and were stacked to form a channel. Each ring was rotated with respect to the previous one to place carbons and oxygens on top of each other. The radius of the channels in the narrow regions was 0.18 nm. The average interplane distance was centered at 0.32 nm. Both the radius and interplane distances guarantee a single-file channel. The shortest ring channel contained two rings, r-02, and was elongated in steps of two rings until r-20, spanning a length range of ~0.5 nm to ~7 nm. All atoms in the channel were restrained by strong position restraints (4000 kJ/mol/nm^2). An artificial membrane was constructed around the channel by position-restraining argon atoms in their *xy* plane (Fig. 1 *b″*), which was constructed normal to the channel main axis. This approach also guarantees a perfect match between the membrane thickness and the channel. We used constant volume simulations for these systems.

The same ring-structured channel setup was used to study the effect of polarity on free energy barriers for ion permeation. Charges were augmented by −0.2 e and +0.2 e for oxygen and carbon, respectively, and the force constant for restraining the atom *z* position was decreased from 4000 kJ/mol/nm^2 to 500 kJ/mol/nm^2. We refer to these systems as ring-07.

The systems were solvated (~1200 water molecules) and KCl was added to achieve a 150-mM concentration. All systems were energy-minimized and simulated at 300 K for 20 ns. The first 2 ns were discarded for equilibration.

Interactions among all atoms of the peptides, ring channels, and membrane were described by means of the OPLS all-atom force field (25,26), and water molecules were described by the TIP4P model (27). Potassium and chloride ion parameters were taken from Åqvist (28), and Chandrasekhar et al. (29), respectively. Parameters for oxygen and carbon atoms in the ring-structured channels ring-05 were assigned as peptide carbonyl atom types, taken from the OPLS all-atom force field. The charges were increased from ±0.5 e to ±0.7 e for the ring-07 channels, as previously explained. All simulations were performed using the GROMACS 3.3.1 simulation software (30,31). Electrostatic interactions were calculated at every step with the particle-mesh Ewald method (32,33). Short-range repulsive and attractive dispersion interactions were simultaneously described by a Lennard-Jones potential, which was cut off at 1.0 nm. The SETTLE (34) algorithm was used to constrain bond lengths and angles of water molecules, and LINCS (35) was used for all other bonds, allowing a time step of 2 fs. The temperature was kept constant by weakly coupling the system to an external heat bath (36) (time constant $\tau = 0.1$ ps). For the constant pressure simulations, a weak semiisotropic coupling to a pressure bath of 1 atm was applied ($\tau = 1$ ps).

PMF computation for ion permeation

Umbrella sampling (US) (37) simulations were applied to obtain biased position histograms along the ion reaction coordinate. The reaction coordinate was defined as the principal axis of the channel, constructed to be the *z* axis of the simulation box. The reaction coordinate was divided in equidistant windows separated by 0.01 nm. To select starting configurations for the US, the equilibrium trajectories of 20 ns were used. For each window, a water molecule in the nearest vicinity of the target position was selected and exchanged by a potassium ion. After energy minimization, the system was ready for the production run.

During the umbrella simulation, a harmonic potential of 4000 kJ/mol/nm^2 was applied on the ion along the reaction coordinate. To ensure complete

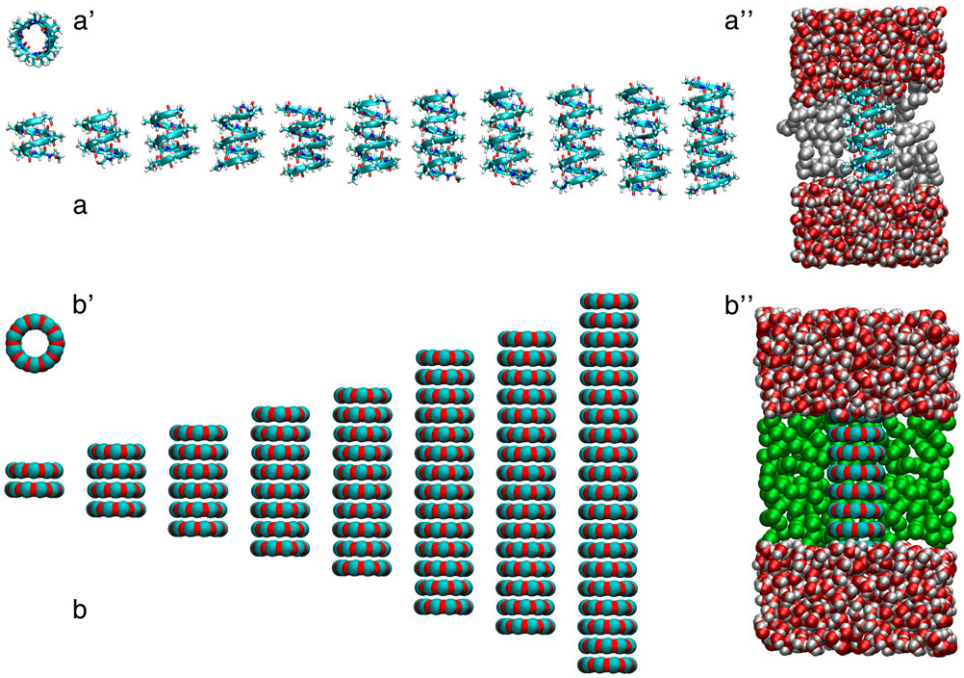

FIGURE 1 Schematic representations of model channels used for the study. (*a*) Side view of polyalanine pores of increasing number of residues, p-11 to p-29. (*a′*) Top view of p-17 channel. (*a″*) Side view of a typical simulation box for polyalanine channels. Half of the octane layer has been omitted for clarity. (*b*) Side view of ring-structured channels of increasing number of rings. (*b′*) Top view of r-02. (*b″*) Simulation box for r-08; half the argon atoms were removed for clarity.

sampling on the ion's plane normal to the reaction coordinate, as well as a well-defined concentration of channels, a cylindrical potential was implemented. A repulsive force $F(r) = -k_c(r - r_c)H(r - r_c)$ on the ion, normal to the reaction coordinate, restrained the ion to a cylinder of radius $r_c = 0.5$ nm, whose axis was centered along the pore. Here, r denotes the distance from the cylinder axis, $k_c = 400$ kJ/mol/nm^2 the force constant, and H the Heaviside step function.

Each umbrella window was simulated for 600 ps in its corresponding ensemble (NPT for polyalanine channels and NVT for ring-structured channels). For the analysis, the first 100 ps were discarded as equilibration. To recover the unbiased position probability distribution, the weighted histogram analysis method (WHAM) (38) was employed. The WHAM equations were iterated until a tolerance of 10^{-6} for the unbiased probability distribution was achieved. To account for the periodicity of the system, a cyclic version of WHAM was implemented. The PMF was obtained from the unbiased position probability distribution $p(z)$, as $-k_BT \ln p(z)$.

Statistical errors of the PMF profile were computed using bootstrap analysis. From N histograms available, N histograms were randomly selected (allowing duplication) and used in a subsequent WHAM procedure. We constrained the random selection of histograms to sample the complete reaction coordinate, avoiding gaps. We considered only complete histograms as independent data points, yielding a rather conservative estimation for the uncertainty. Bootstrapping was done 50 times, yielding 50 PMFs for each channel. From the 50 PMFs, standard deviations were calculated. The uncertainty was generally $\leq$1.5 kJ/mol.

Decomposing PMF features in polyalanine channels

The PMFs for ion permeation through polyalanine channels can be separated in contributions from an entrance barrier and a central barrier which increases with channel length (Fig. 2). Each PMF for the polyalanine channels was decomposed in three overlapping Gaussians. To reduce the number of fitting parameters, p-29 was used to extract the height of the Gaussian located at the entrance barrier. This was done by a free fit (9 parameters) of three Gaussians, centered around the channel lumen and channel entrances. The height of the fitted Gaussian corresponding to the pore entrance for p-29 was then used as a constraint in the multi-Gaussian fit for the rest of the polyalanine PMFs. From these constrained fits, the height of the central barrier was obtained as the height of the central Gaussian.

Computing water dipoles

From four independent 8-ns MD simulations for each channel, we extracted time-averaged position-dependent dipole moments of water molecules inside the pore (Fig. 7). During these simulations, the ion was harmonically restrained at the center of the channel. The water dipole was normalized with respect to the total dipole of the TIP4P water model (2.177 debye).

Extracting entropic and enthalpic contributions to the free energy

To gain insight into the thermodynamic nature of ion permeation barriers in the model channels, we extracted the enthalpic and entropic components of the free energy barriers for ion permeation (Figs. 4 and 6). In contrast to the wealth of techniques to obtain free energies (39–41), the number of methods for calculating enthalpic and entropic contributions of a fully hydrated system is rather limited.

A direct calculation of the enthalpic penalty for ion permeation is complicated by the large energy fluctuations intrinsic in molecular dynamics simulations of thousands of particles. Nevertheless, one can compute time-averaged potential energies for defined configurations of the system of interest. In this work, only the polyalanine channels rendered statistically converged estimates for the enthalpy by this approach. Enthalpy contributions were extracted by harmonically restraining the ion in the highest energetic position of the PMF and in the bulk. The ion in the bulk was fixed 1.4 nm from the pore entrance for all channels. For each channel and ion position, five simulations of 10 ns were performed under the same simulation conditions as in the US runs. After discarding the first 1 ns, the enthalpy of the system in that particular ion configuration was computed as the sum of the potential energy and the pV term (where p is the pressure in the system and V is the volume), corresponding to the enthalpy in an isothermal-isobaric ensemble. The contribution from the position restraint energy was removed from the estimate. The enthalpy difference for each channel, ΔH, was computed as $H_{K^+\text{pore}} - H_{K^+\text{bulk}}$, using averaged values from the 10 independent simulations.

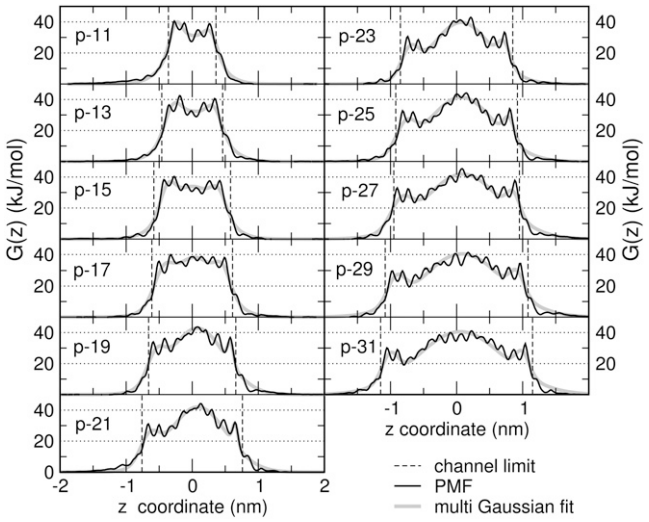

FIGURE 2 Potentials of mean force (PMF) for potassium ion permeation at 300 K for the series of polyalanine peptides (*black*). Underlying each PMF is a three-Gaussian fit to the main features of the channel (*gray*): the two entrance barriers (*constant*) and the central barrier that varies with channel length. Dashed black lines indicate the channel entrance and exit. Errors bars (not shown for clarity) are $<\pm$1.5 kJ/mol.

To compute entropy differences, several strategies (42,43) have been proposed to circumvent the sampling problem of direct entropy calculation. Regrettably, methods that compute ΔS via thermodynamic integration converged too slowly for our systems.

Instead, ΔS was computed via the temperature derivative of the free energy barrier at constant pressure and number of particles N,

$$\Delta S = -\left(\frac{\partial \Delta G}{\partial T}\right)_{N,p}. \quad (1)$$

The former expression is exact, but requires a partial derivative to be evaluated. The partial derivative was approximated by the total derivative, $(d\Delta G/dT)_{N,p}$, assuming a constant heat capacity difference in the simulated temperature range, $(\partial \Delta H/\partial T)_{N,p} \approx 0$. The validity of this approximation was checked by computing ΔH and ΔG independently. If the difference of these two values equals the $-T\Delta S$ result obtained by means of Eq. 1, it implies that the approximation of constant heat capacity difference to compute ΔS is justified.

PMFs were computed at temperatures ranging from 280 K to 320 K in steps of 10 K using US simulations as described earlier. This implies four additional US simulations for each studied channel. To reduce the computational effort, only four representative channels of the polyalanine and four of the ring-structured series were analyzed. From $\Delta G(T)$, ΔS was computed by a weighted linear least-square fit. The weights were chosen according to the statistical uncertainty derived by bootstrap analysis of the PMFs. The statistical error for the entropy estimate was extracted from the uncertainty in the slope of the fitted line. The correlation coefficient was generally $\sim$0.9.

To a first approximation, the entropic contribution due to rotation of water molecules inside the pore was estimated by considering the position-dependent rotational probability distribution, $\rho_{rot}(z)$, of n independent water molecules inside the channel. From $\rho_{rot}(z)$, the rotational entropy was computed along the pore length L as $S_{rot} = -k_B \int_L dz \rho_{rot}(z) \ln \rho_{rot}(z)$. To compute the entropy difference, a system without the ion in the channel was used as the reference state.

We used the Schlitter (44) formula and the quasi-harmonic approximation of Andricioaei and Karplus (45) to estimate the channel entropy based on atomic fluctuations. Both represent an upper bound for the entropy, but they serve to gain a qualitative picture.

To evaluate these rotational and conformational entropies, estimates for eight representative channels (p-15, p-19, p-25, and p-29 for the polyalanine channels; r-04, r-08, r-14, and r-20 for the ring-05 systems) were obtained from two simulations of 100 ns, one with the potassium ion restrained in the center of the channel and one with the ion outside the channel.

RESULTS AND DISCUSSION

The PMFs for potassium ion permeation through the complete series of polyalanine channels are displayed in Fig. 2. The average barrier for ion permeation is ~40 kJ/mol, which is approximately the same free energy barrier reported for gramicidin A embedded in dimyristoylphosphatidylcholine in the absence of finite size, periodicity, and membrane polarizability corrections (22,46). It is known that the lack of electronic polarizability in force fields for lipid membranes, and for octane molecules, leads to an overestimation of the free energy barrier for ion permeation (46,47). Because we are primarily interested in the relative free energy barriers for ion permeation, and membrane polarization effects are not coupled to ion-pore interactions (48), no correction was applied.

The profiles present distinct entrance barriers due to the capping groups and the loss of ion solvation. A local minimum, with a binding energy of ~3 kJ/mol, is located on top of these barriers due to the stabilizing effect of capping groups and the peptide carbonyl charge distribution. Several other binding sites are found along the profiles, resulting from the combinations of ion-peptide and water-peptide interactions.

The overall free energy barrier increases only slightly with increasing channel length, with 5 kJ/mol as the largest difference among the barriers. Further inspection reveals that as the peptidic channel elongates, a central barrier emerges while the entrance barriers decrease, as shown in Fig. 3 *a*. Considering a central barrier that increases with the length of the channel, the entrance barriers appear to be added on top of this more general feature. Decomposition of the different PMFs (see Theory and Methods) clearly shows the rise of the central barrier until saturation (*gray curves* in Fig. 2, *black curve* in Fig. 3). Such a saturation is predicted by continuum theories (49–52) and it corresponds to the self-image potential (free energy in our case) at infinitely long pores.

For ions in the central position, elongating the channel implies a decrease of the long-ranged electrostatic stabilization of the ion provided by the bulk water. Eventually, the presence of bulk water becomes unnoticeable for the ion, and

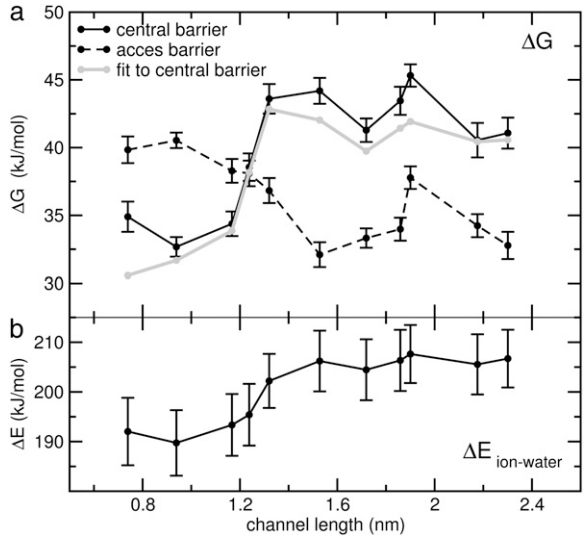

FIGURE 3 Free energy barriers (*a*) for ion permeation in polyalanine channels as a function of channel length. The black line in the upper panel indicates the central barrier ΔG, which is dominant in channels longer than p-17. The height of the central Gaussian function fit (see Theory and Methods for details) is displayed in gray. Dashed lines represent the free energy for the access barrier. The difference in ion-water interaction between the ion in the bulk and the ion inside the center of the channel (*b*) as a function of channel length correlates with the free energy barrier.

the increasingly destabilizing desolvation effect levels-off. The difference between the ion-water potential energy for the ion in bulk and the ion in the channel saturates after p-19 (see Fig. 3 *b*), correlating with the saturation of the free energy barrier. As previously noted (53), ion-channel interactions, together with the stabilization of the ion by the single-file water column, are not able to fully compensate for the loss of the ion's solvation shell.

Construction of the enthalpy barrier for ion permeation from contributions of the different constituents (water-water, water-ion, ion-pore...) is in principle possible, but challenging due to the large compensating energy terms involved. Instead, we extracted the complete enthalpy contribution to the free energy (Fig. 4 *a*, *dashed curve*) using four representative channels (p-15, p-19, p-25, and p-29) as described in Theory and Methods. The averaged values for ΔH show the same saturation trend as the free energy, although subject to large fluctuations, that is responsible for ~5 kJ/mol uncertainty. Entropy estimates, based on temperature dependence of the PMF, reflect a similar tendency, but also suffer from statistical inaccuracy (Fig. 4 *a*, *gray curve*). Nevertheless, the sum of the two individual components ΔH and $-T\Delta S$ agrees well with the free energy extracted from umbrella sampling, justifying the use of Eq. 1. The parallel saturation of the enthalpy and the ion-water desolvation energy with the channel length indicates that the enthalpy strongly contributes to length dependence of the free energy. Remarkably, there is a reduction of the system entropy when the ion is moved from the bulk to the channel center. Furthermore, the

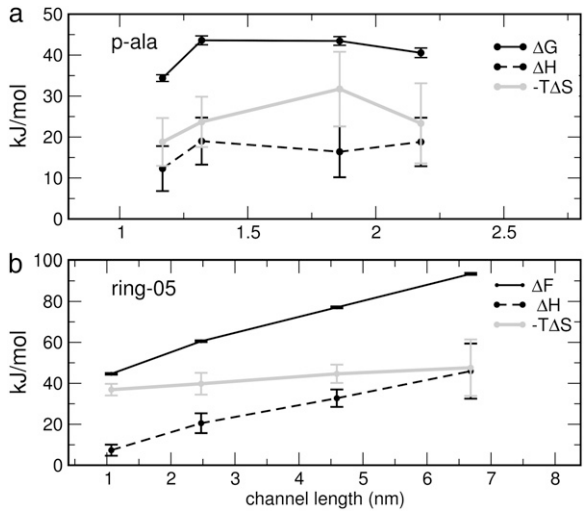

FIGURE 4 Decomposition of free energy barriers for potassium ion permeation through polyalanine (*a*) and ring-05 (*b*) selected channels. The entropy components are weighted with the temperature (300 K) and sign reversed ($-T\Delta S$). For the polyalanine channels, all thermodynamic quantities could be directly computed from the simulation. For the ring-structured channel with charges ± 0.5 *e*, only the free energies and the entropies could be extracted independently from the umbrella simulations. The enthalpy contribution of the ring system was computed from $\Delta H = \Delta G + T\Delta S$.

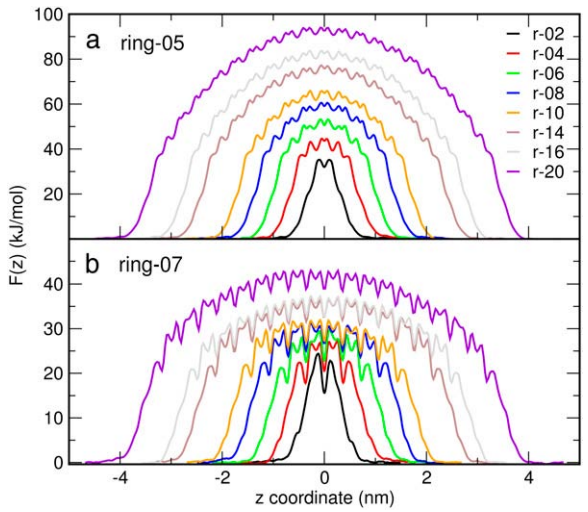

FIGURE 5 PMFs, $F(z)$, for potassium ion permeation through ring-structured channels. (*a*) PMFs for ring channels with charges of $+0.5$ *e* on the carbon and -0.5 *e* on the oxygen. (*b*) PMFs for ring channels with charges of $+0.7$ *e* on the carbon, -0.7 e on the oxygen, and increased flexibility along the *z* coordinate.

entropy contributes more to the total free energy barrier than the enthalpy. This results contrasts with the entropy-enthalpy compensating effects found in many aqueous systems (54–56). Such large contribution to the free energy was speculated by Jordan (57,58), who assigned the effect to the low probability of concerted motions in single-file channels. The reduction of the entropy of the system is directly connected to an increase of the free energy barrier with the temperature, via Eq. 1. Note that this does not imply a decrease of the ion flux with temperature, i.e., an inverse Arrhenius plot. Although the activation free energy required increases with temperature, the ratio $\Delta G(T)/T$ decreases, yielding normal Arrhenius behavior.

Ring-structured channels

To isolate the influence of the capping groups and hence to focus on the effect of ion desolvation, we investigated more simplified channels (see Fig. 1 *b*). Fig. 5 *a* shows the sequence of PMF profiles for artificial channels of increasing numbers of rings (r-02 to r-20). Here we denote the free energies as *F*, since the use of constant volume simulations results in Helmholtz free energies. After a sharp rise of the PMF at the channel entrance, there is a systematic concave increase of the free energy until the ion reaches the central position. Local minima inside the channel correspond to the position of the rings, whereas local maxima are found between ring planes. Fig. 6 *a* (*black curve*) displays the overall free energy barrier, which, surprisingly, increases approximately linearly with the channel length. This is remarkable, since r-20 is 6.6-nm-long—roughly three times longer than p-ala29, where a saturation was observed. The ΔH contribution to the free energy (Fig. 4 *b*), which includes the resulting cancellations of large interaction components, shows an almost linear increase, parallel to the free energy versus the channel length. Since the desolvation penalty for ion permeation, as monitored via ion-water interaction (Fig. 6 *b*, *black curve*), does saturate at approximately r-10, the overall enthalpy increase is attributed to the water-water and water-channel components of the enthalpy. As for the polyalanine channels described above, we used four representative channels (r-04, r-08, r-14, and r-20) to extract the enthalpy and the entropy terms that account for the free energy barriers. Like the polyalanine channels, the entropy reduction dominates the free energy barrier. This effect is maximal for the shorter channels, but does not increase as fast as the enthalpic penalty.

Free energy barriers were found to be higher in the ring-05 channels than for the polyalanine channels, due to the low polarity. A second set of ring channels (ring-07, see Theory and Methods) with augmented charges and larger mobility along the *z* axis showed much lower barriers (Fig. 4 *a*, *dashed curve*). Extraction of the ion-water potential energy reveals very similar values to those obtained for the ring-05 channels (Fig. 4 *b*, *dashed curve*). Therefore, the higher interaction energy between ion-channel and water-channel is likely responsible for the reduction of free energy barriers.

From the thermodynamic analysis performed on the two types of channels, polyalanine and ring systems, we conclude that the length dependence of the free energy is strongly influenced by the enthalpy, but the major contribution to the free energy is entropic.

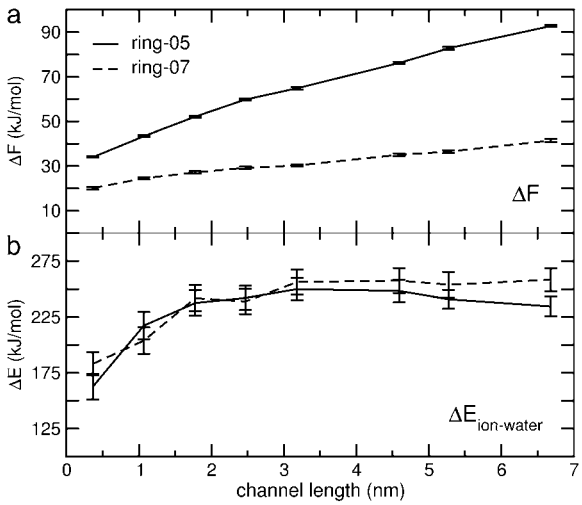

FIGURE 6 Free energy barriers, ΔF, (*a*) and ion-water potential energy difference between the bulk and the channel (*b*) for the ring-structured channels, as a function of channel length.

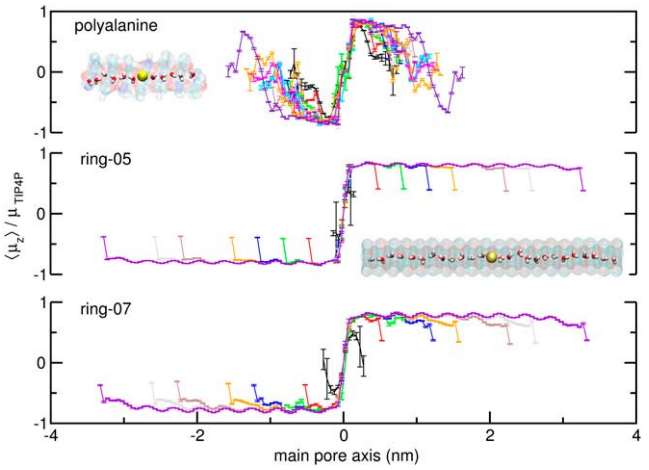

FIGURE 7 Projection of the average dipole moment, $\langle \mu_z \rangle$, of water molecules inside the channel onto the pore axis for the polyalanine channels (*upper panel*), the ring-05 (*center*), and the ring-07 (*lower panel*) channels. The water dipole was normalized with respect to the total dipole of the TIP4P water model (2.177 debye). Different colors indicate different channels of increasing length. Profiles have been symmetrized. On the upper left, a typical simulation snapshot shows the water orientation when the ion (*yellow sphere*) occupies the central position. As seen from the $\langle \mu_z \rangle$ curves, water molecules far from the ion lose their alignment with the pore axis in the polyalanine channels due to a decay of the electric field and interactions with the bulk water (not shown). The central and lower panels illustrate the long-ranging polarization induced by the potassium ion for the ring channels.

Origin of entropic barriers

Now that we have established the role of entropy, it is interesting to see which parts of the system contribute most to this entropic cost. There are two components that lead to a significant increase of the system entropy when moving an ion from the bulk to the center of the channel: 1), removing a potassium ion from the bulk, ~17 kJ/mol for a potassium ion at 300 K (59); and 2), moving a water molecule from the channel to the bulk to allocate the ion in the channel. Since the overall system entropy decreases, this gain in entropy must be surpassed by entropy-reducing effects. The entropic cost for an ion to find the channel, which depends on the density of channels in the membrane, is $T\Delta S_{\mathrm{dens}} = k_{\mathrm{B}}T \ln(A_{\mathrm{in}}/A_{\mathrm{out}})$, where A_{out} is the membrane area per channel and A_{in} is the area along the membrane plane available for an ion inside the pore. The radius of the cylindrical potential, r_{c}, used to ensure a well-defined channel concentration, is approximately twice the effective pore radius, which in the simulated conditions corresponds to a ΔS_{dens} of only ~1.7 kJ/mol, which is too small to account for the observed entropy reduction. In the following, we discuss the reduction of rotational entropy for water in the channel and restrictions of channel mobility upon ion binding as the major components.

Fig. 7 displays the normalized averaged projection of water dipoles onto the pore axis ($\langle \mu_z \rangle$) for all studied channels as function of their position in the pore. For the polyalanine pores, the influence of the electric field drops quickly after the first two water molecules around the ion. In the ring systems, the long-ranged ordering of water molecules reveals that the electric field propagates further through the single-file. Increasing the polarity and mobility of the channel reduces the extent of water dipole ordering, as seen in the ring-07 averaged dipole projection near the bulk interface. Due to the imposed ordering of water molecules caused by the ion, the rotational entropy of water molecules in the channel is reduced. We used the first-order uncorrelated rotational probability density (see Theory and Methods) as a crude estimate for the entropy reduction of water molecules inside the channel. Considering the water occupancy for each channel, the contribution to the entropy for polyalanine channels in terms of energetic cost ($-T\Delta S$) ranges from 10 (p-15) to 18 kJ/mol (p-29), and from 15 (r-04) to 55 kJ/mol (r-20) for the ring-05 system. Note that these values can only be interpreted qualitatively because of the severe assumptions underlying these estimates.

The electrostatic interactions between the channel and the permeating ion cause a significant effect on the mobility of the pore. For the polyalanine channels, the loss of the corresponding conformational channel entropy at 300 K ranges from 10 (p-15) to 28 kJ/mol (p-29), and it extends between 14 (r-04) and 25 kJ/mol (r-20) for the ring-05 channels. Entropies computed using the Schlitter formula and quasi-harmonic approximation agree within 0.2 kJ/mol.

The entropic contributions presented are an upper bound, but they provide a strong indication that channel mobility and rotational water freedom in the channel are reduced in the presence of the ion in its lumen, which leads to an overall system entropy reduction upon ion permeation.

Finally, it is of interest to compare these results with experimental findings and to discuss the implications for biological channels and the design of novel channels. The selectivity filter of naturally occurring channels, such as the

bacterial potassium channel KcsA, is shorter (1.2 nm in length (4)) than the lipid bilayer in which it is embedded. Apart from ion stabilizing helical dipoles and multiple ion occupancies (4,60–63), a short selectivity filter contributes to the high ion rate (3).

Qualitative agreement with experimental ion flux through single-file channels of different length can be found in ion conductance through gramicidin A derivatives minigramicidin and midigramicidin (64). In 1 mM KCl solution, embedded in a mixture of dimyristoylphosphatidylcholine and *Escherichia coli* lipid extract, minigramicidin, ~1.8 nm in length, has a conductance of 0.27 pS, and midigramicidin, ~2-nm-long, shows a conductance of 0.20 pS.

To design ion channels for technological applications, the efficiency of ion transport through the channel can be modulated by adapting the single-file length, the polarity, and the flexibility of the pore. Short, polar, and flexible channels will permeate ions at higher rate than long, stiff, apolar channels. Furthermore, since single-file water mobility under osmotic conditions is virtually invariant to the pore length (23,65), long single-file channels would allow fast flow of water molecules while effectively avoiding the passage of ions, thereby shifting the ion/water selectivity. Such length variability and fixed radius can be experimentally implemented, e.g., in carbon nanotubes.

CONCLUSIONS

The influence of the channel length on potassium ion permeation depends on the nature of the channel. Replacement of the solvation shell in bulk cannot be fully compensated by the polar fragments inside the channel and the single-file of water molecules. In peptidic channels, the saturation of the free energy barrier with increasing channel length mainly arises due to parallel saturation of the reduced ion-water interaction. In contrast, more rigid channels with a similar charge distribution fail to stabilize the barrier for ion permeation, leading to a constant increase of the central barrier with the channel length.

A decomposition of the free energies into enthalpic and entropic contributions enabled us to determine the origin of the permeation barriers. In all studied channels, the entropic cost for ion permeation was found to be higher than the enthalpic penalty. Although an increase in the entropy of the water is gained after removing the ion from the bulk, the combination of channel and water mobility reduction lowers the system's entropy as the ion permeates the channel.

The general picture emerging from our study is twofold: while the length dependence is strongly influenced by the enthalpic component of the free energy, a reduction of the system entropy as the ion passes the channel is the major contribution to the permeation barrier.

G.P. was supported by Deutsche Forschungsgemeinschaft grant No. GR-2079/2. J.S.H. was supported by European Union grant No. LSHP-CT-2004-012189.

REFERENCES

1. Wallace, B. A. 2000. Common structural features in gramicidin and other ion channels. *Bioessays.* 22:227–234.
2. Hille, B. 2001. Ion Channels of Excitable Membranes, 3rd Ed. Sinauer, Sunderland, MA.
3. Gouaux, E., and R. Mackinnon. 2005. Principles of selective ion transport in channels and pumps. *Science.* 310:1461–1465.
4. Doyle, D. A., J. M. Cabral, R. A. Pfuetzner, A. L. Kuo, J. M. Gulbis, S. L. Cohen, B. T. Chait, and R. MacKinnon. 1998. The structure of the potassium channel: molecular basis of K^+ conduction and selectivity. *Science.* 280:69–77.
5. Zhou, Y., J. H. Morais-Cabral, A. Kaufman, and R. MacKinnon. 2001. Chemistry of ion coordination and hydration revealed by a K_+ channel-Fab complex at 2.0 Å resolution. *Nature.* 414:43–48.
6. Roux, B. 2005. Ion conduction and selectivity in K^+ channels. *Annu. Rev. Biophys. Biomol. Struct.* 34:153–171.
7. Noskov, S. Y., and B. Roux. 2006. Ion selectivity in potassium channels. *Biophys. Chem.* 124:279–291.
8. Bostick, D. L., and C. L. Brooks. 2007. Selectivity in K^+ channels is due to topological control of the permeant ion's coordinated state. *Proc. Natl. Acad. Sci. USA.* 104:9260–9265.
9. Andersen, O. S. 1984. Gramicidin channels. *Annu. Rev. Physiol.* 46:531–548.
10. Andersen, O. S., and R. E. Koeppe. 1992. Molecular determinants of channel function. *Physiol. Rev.* 72:S89–S158.
11. Futaki, S., Y. J. Zhang, T. Kiwada, I. Nakase, T. Yagami, S. Oiki, and Y. Sugiura. 2004. Gramicidin-based channel systems for the detection of protein-ligand interaction. *Bioorg. Med. Chem.* 12:1343–1350.
12. Antonenko, Y. N., T. I. Rokitskaya, E. A. Kotova, G. O. Reznik, T. Sano, and C. R. Cantor. 2004. Effect of streptavidins with varying biotin binding affinities on the properties of biotinylated gramicidin channels. *Biochemistry.* 43:4575–4582.
13. Capone, R., S. Blake, M. R. Restrepo, J. Yang, and M. Mayer. 2007. Designing nanosensors based on charged derivatives of gramicidin A. *J. Am. Chem. Soc.* 129:9737–9745.
14. Beckstein, O., and M. S. P. Sansom. 2004. The influence of geometry, surface character, and flexibility on the permeation of ions and water through biological pores. *Phys. Biol.* 1:42–52.
15. Peter, C., and G. Hummer. 2005. Ion transport through membrane-spanning nanopores studied by molecular dynamics simulations and continuum electrostatics calculations. *Biophys. J.* 89:2222–2234.
16. Chung, S. H., and B. Corry. 2005. Three computational methods for studying permeation, selectivity and dynamics in biological ion channels. *Soft Matter.* 1:417–457.
17. Kirkwood, J. G. 1935. Statistical mechanics of fluid mixtures. *J. Chem. Phys.* 3:300–313.
18. Bernèche, S., and B. Roux. 2003. A microscopic view of ion conduction through the K^+ channel. *Proc. Natl. Acad. Sci. USA.* 100:8644–8648.
19. Roux, B., T. W. Allen, S. Bernèche, and W. P. Im. 2004. Theoretical and computational models of biological ion channels. *Q. Rev. Biophys.* 37:15–103.
20. Beckstein, O., K. Tai, and M. S. P. Sansom. 2004. Not ions alone: barriers to ion permeation in nanopores and channels. *J. Am. Chem. Soc.* 126:14694–14695.
21. Allen, T. W., O. S. Andersen, and B. Roux. 2004. On the importance of atomic fluctuations, protein flexibility, and solvent in ion permeation. *J. Gen. Physiol.* 124:679–690.
22. Bastug, T., A. Gray-Weale, S. M. Patra, and S. Kuyucak. 2006. Role of protein flexibility in ion permeation: a case study in gramicidin A. *Biophys. J.* 90:2285–2296.
23. Portella, G., P. Pohl, and B. L. de Groot. 2007. Invariance of single-file water mobility in gramicidin-like peptidic pores as function of pore length. *Biophys. J.* 92:3930–3937.

24. Crozier, P. S., R. L. Rowley, N. B. Holladay, D. Henderson, and D. D. Busath. 2001. Molecular dynamics simulation of continuous current flow through a model biological membrane channel. *Phys. Rev. Lett.* 86:2467–2470.
25. Kaminski, G. A., R. A. Friesner, J. Tirado-Rives, and W. L. Jorgensen. 2001. Evaluation and reparameterization of the OPLS-AA force field for proteins via comparison with accurate quantum chemical calculations on peptides. *J. Phys. Chem. B.* 105:6474–6487.
26. Jorgensen, W. L., D. S. Maxwell, and J. Tirado-Rives. 1996. Development and testing of the OPLS all-atom force field on conformational energetics and properties of organic liquids. *J. Am. Chem. Soc.* 118:11225–11236.
27. Jorgensen, W. L., J. Chandrasekhar, J. D. Madura, R. W. Impey, and M. L. Klein. 1983. Comparison of simple potential functions for simulating liquid water. *J. Chem. Phys.* 79:926–935.
28. Aqvist, J. 1990. Ion-water interaction potentials derived from free energy perturbation simulations. *J. Phys. Chem.* 94:8021:8024.
29. Chandrasekhar, J., D. C. Spellmeyer, and W. L. Jorgensen. 1984. Energy component analysis for dilute aqueous solutions of lithium(1+), sodium(1+), fluoride(1-), and chloride(1-) ions. *J. Am. Chem. Soc.* 106:903–910.
30. Lindahl, E., B. Hess, and D. Van der Spoel. 2001. GROMACS 3.0: a package for molecular simulation and trajectory analysis. *J. Mol. Model.* 7:306–317.
31. Van der Spoel, D., E. Lindahl, B. Hess, G. Groenhof, A. E. Mark, and H. J. C. Berendsen. 2005. GROMACS: fast, flexible and free. *J. Comput. Chem.* 26:1701–1718.
32. Darden, T., D. York, and L. Pedersen. 1993. Particle mesh Ewald: an $N\cdot\log(N)$ method for Ewald sums in large systems. *J. Chem. Phys.* 98:10089–10092.
33. Essmann, U., L. Perera, M. L. Berkowitz, T. Darden, H. Lee, and L. G. Pedersen. 1995. A smooth particle mesh Ewald potential. *J. Chem. Phys.* 103:8577–8592.
34. Miyamoto, S., and P. A. Kollman. 1992. SETTLE: an analytical version of the SHAKE and RATTLE algorithms for rigid water models. *J. Comput. Chem.* 13:952–962.
35. Hess, B., H. Bekker, H. J. C. Berendsen, and J. G. E. M. Fraaije. 1997. LINCS: a linear constraint solver for molecular simulations. *J. Comput. Chem.* 18:1463–1472.
36. Berendsen, H. J. C., J. P. M. Postma, A. DiNola, and J. R. Haak. 1984. Molecular dynamics with coupling to an external bath. *J. Chem. Phys.* 81:3684–3690.
37. Torrie, G. M., and J. P. Valleau. 1974. Monte Carlo free energy estimates using non-Boltzmann sampling: application to the subcritical Lennard-Jones fluid. *Chem. Phys. Lett.* 28:578–581.
38. Kumar, S., D. Bouzida, R. H. Swendsen, P. A. Kollman, and J. M. Rosenberg. 1992. The weighted histogram analysis method for free-energy calculations on biomolecules. I. The method. *J. Comput. Chem.* 13:1011–1021.
39. Beveridge, D. L., and F. M. DiCapua. 1989. Free energy via molecular simulation: applications to chemical and biomolecular systems. *Annu. Rev. Biophys. Biophys. Chem.* 18:431–492.
40. Kollman, P. A. 1993. Free energy calculations: applications to chemical and biochemical phenomena. *Chem. Rev.* 93:2395–2417.
41. Meirovitch, H. 2007. Recent developments in methodologies for calculating the entropy and free energy of biological systems by computer simulation. *Curr. Opin. Struct. Biol.* 17:181–186.
42. Peter, C., C. Oostenbrink, A. van Dorp, and W. F. van Gunsteren. 2004. Estimating entropies from molecular dynamics simulations. *J. Chem. Phys.* 120:2652–2661.
43. Wan, S., R. H. Stote, and M. Karplus. 2004. Calculation of the aqueous solvation energy and entropy, as well as free energy, of simple polar solutes. *J. Chem. Phys.* 121:9539–9548.
44. Schlitter, J. 1993. Estimation of absolute and relative entropies of macromolecules using the covariance matrix. *Chem. Phys. Lett.* 215: 617–621.
45. Andricioaei, I., and M. Karplus. 2001. On the calculation of entropy from covariance matrices of the atomic fluctuations. *J. Chem. Phys.* 115:6289–6292.
46. Allen, T. W., O. S. Andersen, and B. Roux. 2006. Ion permeation through a narrow channel: using gramicidin to ascertain all-atom molecular dynamics potential of mean force methodology and biomolecular force fields. *Biophys. J.* 90:3447–3468.
47. Aqvist, J., and A. Warshel. 1989. Energetics of ion permeation through membrane channels. Solvation of Na^+ by gramicidin A. *Biophys. J.* 56:171–182.
48. Roux, B. 1999. Statistical mechanical equilibrium theory of selective ion channels. *Biophys. J.* 77:139–153.
49. Parsegian, A. 1969. Energy of an ion crossing a low dielectric membrane: solutions to four relevant electrostatic problems. *Nature.* 221:844–846.
50. Levitt, D. G. 1978. Electrostatic calculations for an ion channel. I. Energy and potential profiles and interactions between ions. *Biophys. J.* 22:209–219.
51. Jordan, P. C. 1982. Electrostatic modeling of ion pores. Energy barriers and electric field profiles. *Biophys. J.* 39:157–164.
52. Teber, S. 2005. Translocation energy of ions in nano-channels of cell membranes. *J. Stat. Mech.* 7:1–17.
53. Allen, T. W., O. S. Andersen, and B. Roux. 2003. Energetics of ion conduction through the gramicidin channel. *Proc. Natl. Acad. Sci. USA.* 101:117–122.
54. Sharp, K. 2001. Entropy–enthalpy compensation: fact or artifact? *Protein Sci.* 10:661–667.
55. van der Vegt, N. F., D. Trzesniak, B. Kasumaj, and W. F. van Gunsteren. 2004. Energy-entropy compensation in the transfer of nonpolar solutes from water to cosolvent/water mixtures. *ChemPhysChem.* 5:144–147.
56. Ozal, T. A., and N. F. A. van der Vegt. 2006. Confusing cause and effect: energy-entropy compensation in the preferential solvation of a nonpolar solute in dimethyl sulfoxide/water mixtures. *J. Phys. Chem. B.* 110:12104–12112.
57. Jordan, P. C. 1984. Total electrostatic potential in a gramicidin channel. *J. Membr. Biol.* 78:91–102.
58. Jordan, P. C. 1999. Ion permeation and chemical kinetics. *J. Gen. Physiol.* 114:601–603.
59. Lynden-Bell, R. M., and J. C. Rasaiah. 1997. From hydrophobic to hydrophilic behavior: a simulation study of solvation entropy and free energy of simple solutes. *J. Chem. Phys.* 107:1981–1991.
60. Roux, B., and R. MacKinnon. 1999. The cavity and pore helices in the KcsA K^+ channel: electrostatic stabilization of monovalent cations. *Science.* 285:100–102.
61. Shrivastava, I. H., and M. S. P. Sansom. 2000. Simulations of ion permeation through a potassium channel: molecular dynamics of KcsA in a phospholipid bilayer. *Biophys. J.* 78:557–570.
62. Åqvist, J., and V. Luzhkov. 2000. Ion permeation mechanism of the potassium channel. *Nature.* 404:881–884.
63. Berneche, S., and B. Roux. 2001. Energetics of ion conduction through the K^+ channel. *Nature.* 414:73–77.
64. Saparov, S. M., J. R. Pfeifer, L. Al-Momani, G. Portella, B. L. deGroot, U. Koert, and P. Pohl. 2006. Mobility of a one-dimensional confined file of water molecules as a function of file length. *Phys. Rev. Lett.* 96:148101.
65. Kalra, A., S. Garde, and G. Hummer. 2003. Osmotic water transport through carbon nanotube membranes. *Proc. Natl. Acad. Sci. USA.* 100:10175–10180.